Temperature-dependent optical properties of ice crystals in the far-infrared regime

Tong Ren,[1] Ping Yang,[1] Helen E. Brindley,[2] Tristan S. L'Ecuyer[3,4], and Tiziano Maestri[5]

1. Department of Atmospheric Sciences, Texas A&M University, College Station, TX, USA

2. Department of Physics, National Centre for Earth Observation, Imperial College London, Kensington, UK

3. Department of Atmospheric and Oceanic Sciences, University of Wisconsin–Madison, Madison, Wisconsin, USA

4. Center for Climate Research, University of Wisconsin–Madison, Madison, Wisconsin, USA

5. Department of Physics and Astronomy, Università di Bologna, Bologna, Italy

Corresponding author: Tong Ren (tr7585@tamu.edu)

Contents of this file

Text S1

Figures S1 to S10

Table S1

Introduction

The supporting information provided here includes a detailed description of the data smoothing in the development of the temperature-dependent ice aggregate optics database (Text S1) and 10 additional figures. Figure S1 is a flowchart of the development of the temperature-dependent ice aggregate optics dateset and its application to a brightness temperature (BT) simulation study. Figure S2 shows a selected scattering matrix from the ice cloud bulk optical property dataset and associated reconstructed P11 with Legendre polynomials. Figures S3-S6 are same as Figure 2 except for viewing

zenith angles (VZAs) of 15º, 30º, 45º, and 60º, respectively. Figures S7-S10 show variations of computed temperature-dependent ice cloud bulk optical properties at 4 selected wavenumbers. Table 1 documents the settings of ice cloud bulk optical properties in the 3 different radiative transfer experiments.

Text S1.

In this study, at each wavelength (λ), we perform the Invariant Imbedding T-matrix Method (IITM) computation for one more size D_1, which is the smallest maximum dimension (D) satisfying $x \geq 50$, where $x = 2\pi D/\lambda$. The IITM computed extinction efficiency (Q_{ext}) and absorption efficiency (Q_{abs}) at D_1 are used as the reference to quantify the errors of the improved geometric optics method (IGOM) computed Q_{ext} and Q_{abs} ($\Delta Q_{\text{ext}}(D_1, \lambda)$ and $\Delta Q_{\text{abs}}(D_1, \lambda)$). As in Yang et al. (2013), we assume

$$\Delta Q_{\text{ext}}(D, \lambda) = \eta_{\text{ext}}(\lambda)x(D, \lambda)^{-2/3}, \tag{S1}$$

$$\Delta Q_{\text{abs}}(D, \lambda) = \eta_{\text{abs}}(\lambda)x(D, \lambda)^{-2/3}, \tag{S2}$$

where the coefficients $\eta_{\text{ext}}(\lambda)$ and $\eta_{\text{abs}}(\lambda)$ are determined with $\Delta Q_{\text{ext}}(D_1, \lambda)$ and $\Delta Q_{\text{abs}}(D_1, \lambda)$. At each λ and D, the errors $\Delta Q_{\text{ext}}(D, \lambda)$ and $\Delta Q_{\text{abs}}(D, \lambda)$ are subtracted from IGOM computed $Q_{\text{ext}}(D, \lambda)$ and $Q_{\text{abs}}(D, \lambda)$ to complete the edge effect correction.

In addition, while no previous studies have reported this, for some unknown reasons, in the wavelength range between 36.4 and 51.3 μm, when the real part of the refractive index (n) is close to 1 or the imaginary part of the refractive index (k) is large, specifically close to 1, IGOM occasionally computes unrealistic single-scattering albedo and asymmetry factor results for this particle shape. We choose to smooth out the unrealistic data using linear interpolations in the size dimension before the edge effect correction is performed. The same linear interpolations are applied to both the asymmetry factor and scattering phase matrix.
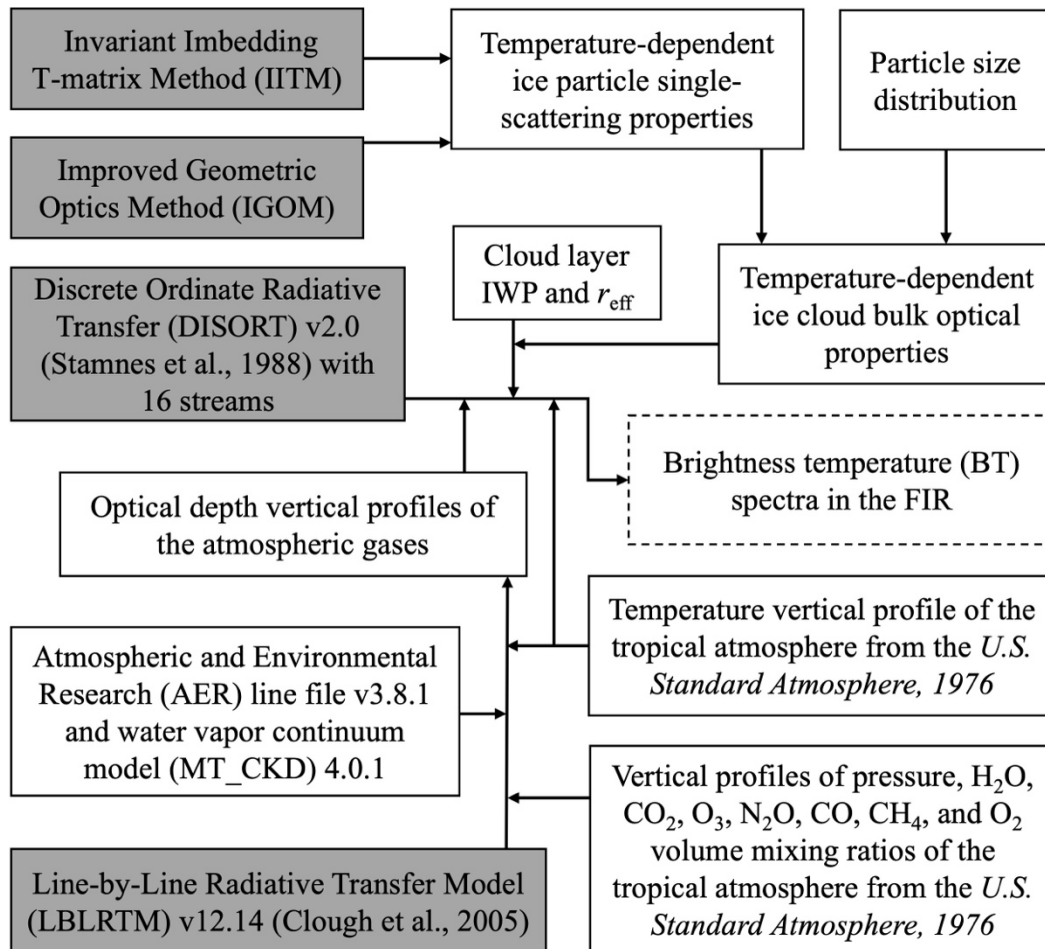
Figure S1. Flowchart of the development of the temperature-dependent ice aggregate optics dateset and its application to a BT simulation study. IWP and r_{eff} are ice water path and cloud effective radius, respectively. FIR is short for far-infrared.
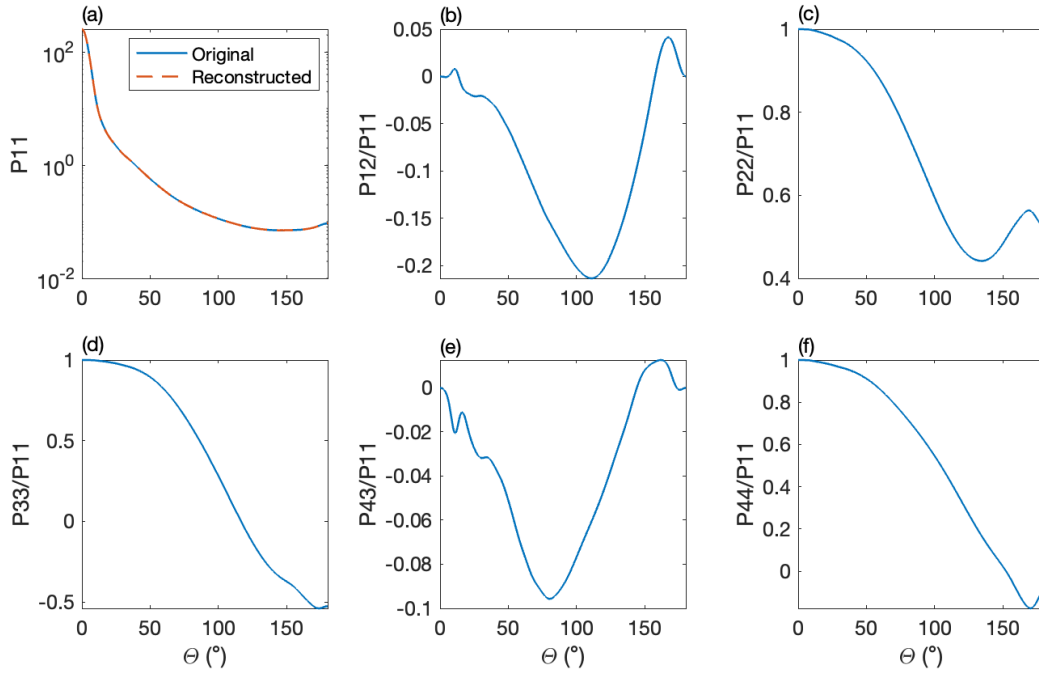
Figure S2. The 6 independent elements in the roughened hexagonal aggregate ice cloud bulk scattering matrix at the temperature of 220 K, the wavelength of 24.8765 μm, and the effective radius of 32.5 μm. Θ is scattering angle; P11, P12, P22, P33, P43, and P44 are the 6 elements in the scattering matrix. The dashed orange curve in panel (a) is the reconstructed P11 with Legendre polynomials up to the 640th order.
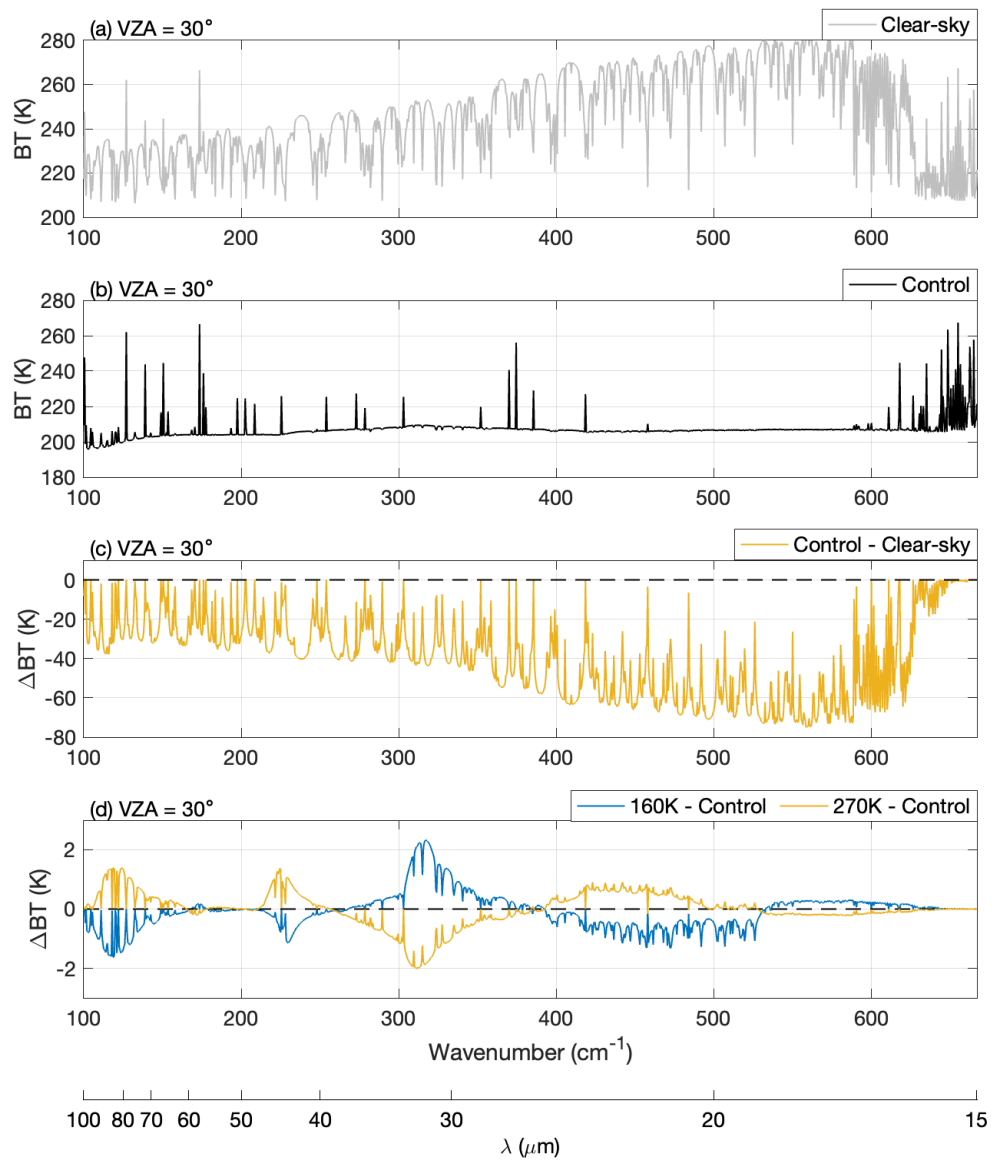
Figure S3. Same as Figure 2 except for VZA = 15º.
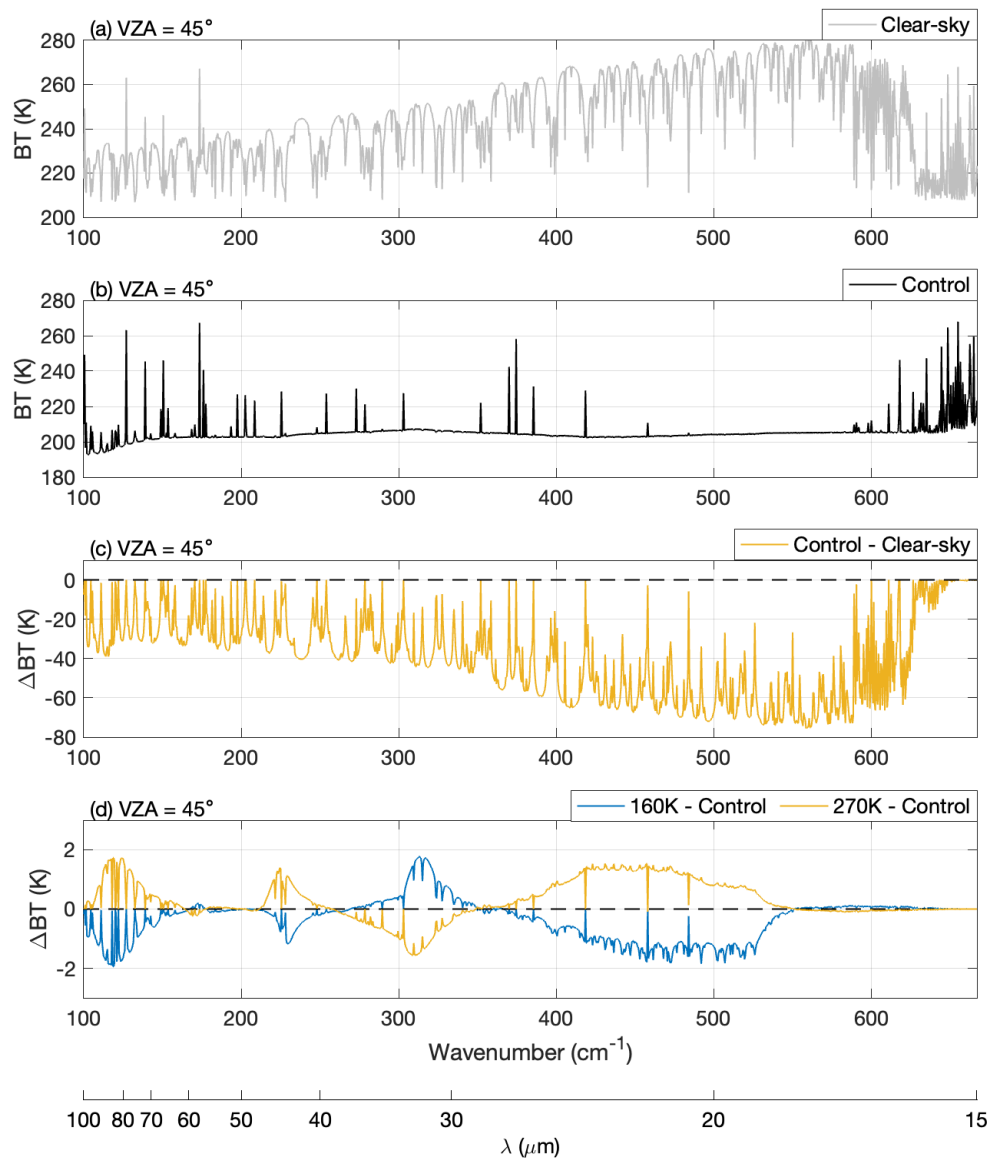
Figure S4. Same as Figure 2 except for VZA = 30º.
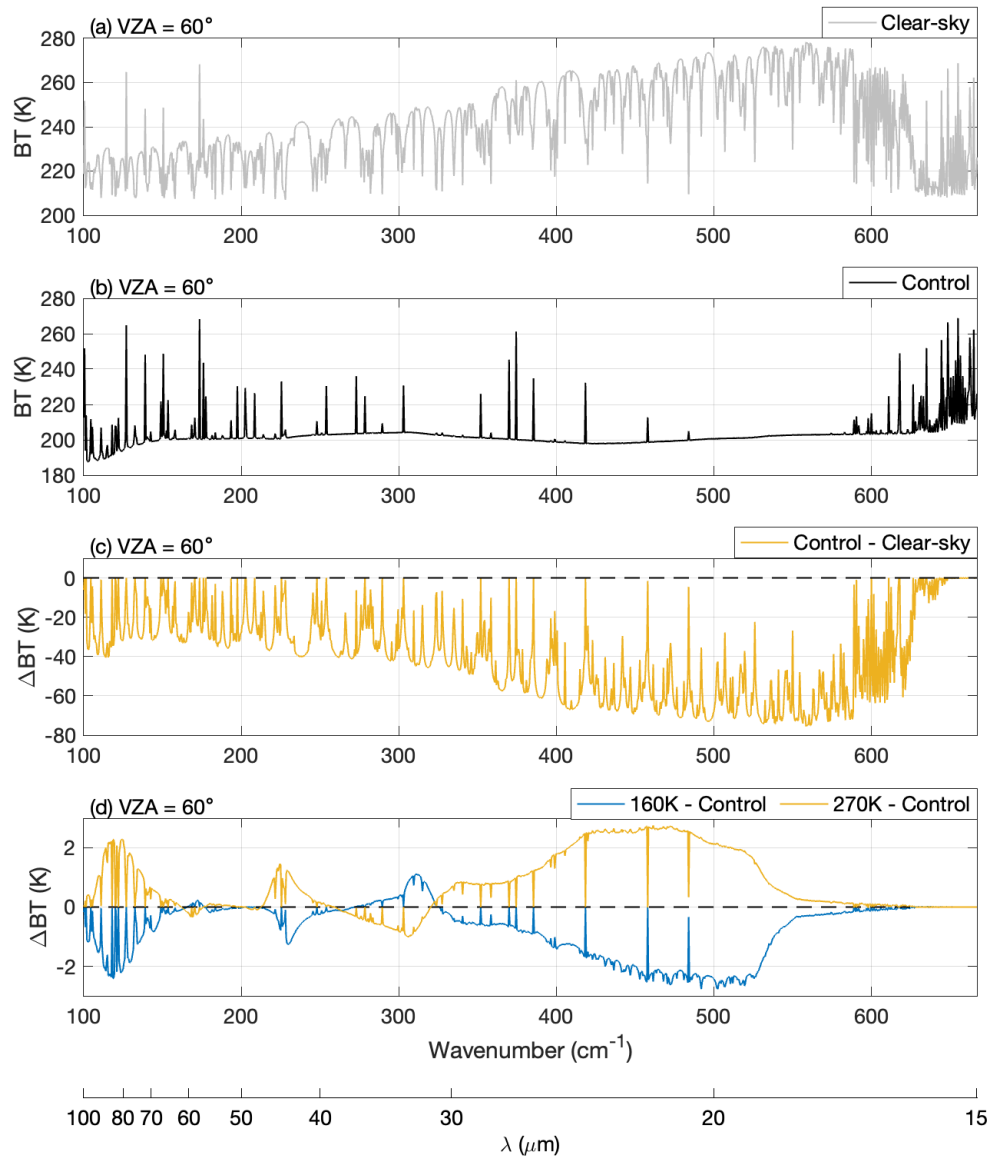
Figure S5. Same as Figure 2 except for VZA = 45º.
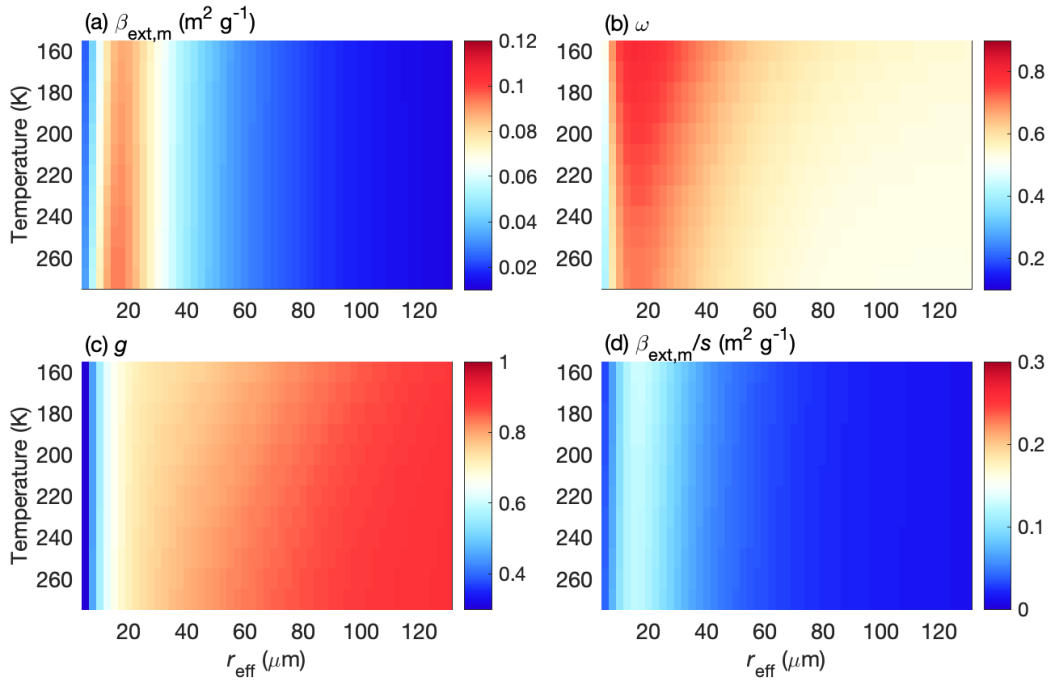
Figure S6. Same as Figure 2 except for VZA = 60º.

Figure S7. Variations of computed ice cloud bulk (a) mass extinction coefficient ($\beta_{\text{ext,m}}$; m^2 g^{-1}), (b) single-scattering albedo (ω), (c) asymmetry factor (g), and (d) ratio of mass extinction coefficient to the similarity parameter ($\beta_{\text{ext,m}}/s$; m^2 g^{-1}) with respect to cloud effective radius (r_{eff}) and temperature at the wavenumber of 120 cm^{-1} (or $\lambda = 83.2518$ μm).
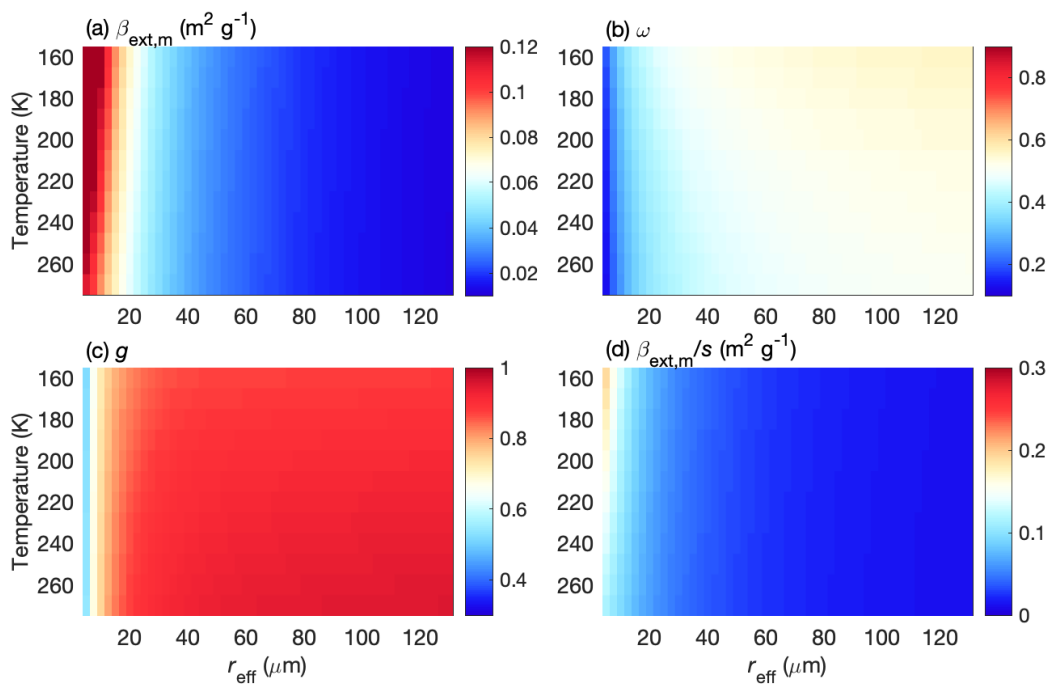
Figure S8. Same as Figure S7 except at the wavenumber of 235 cm^{-1} (or $\lambda = 42.5963$ μm).
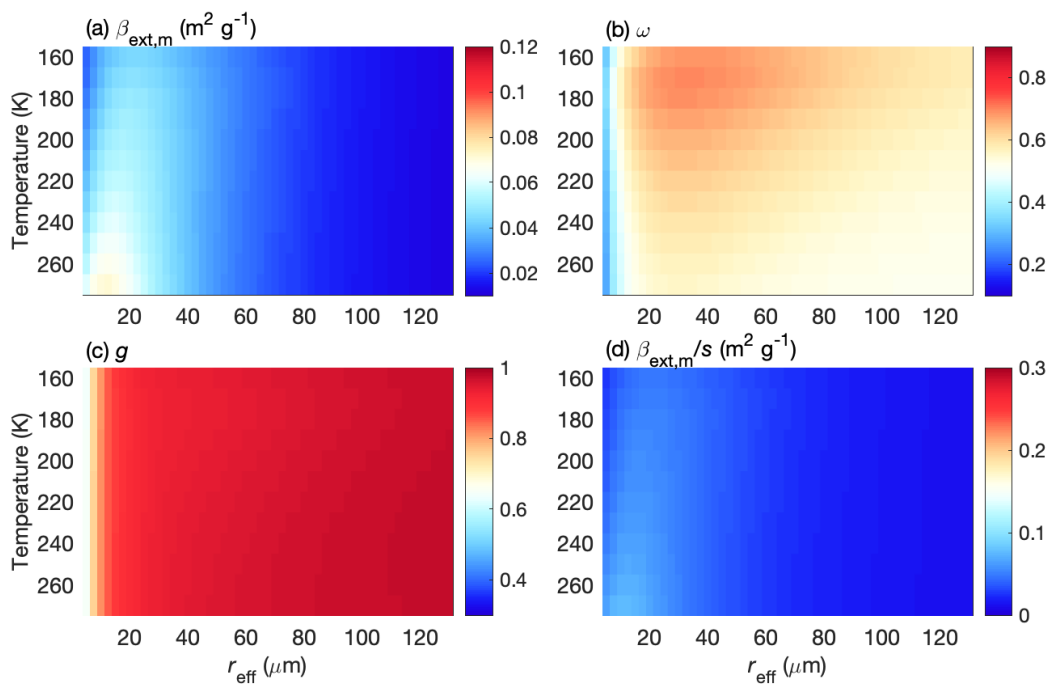
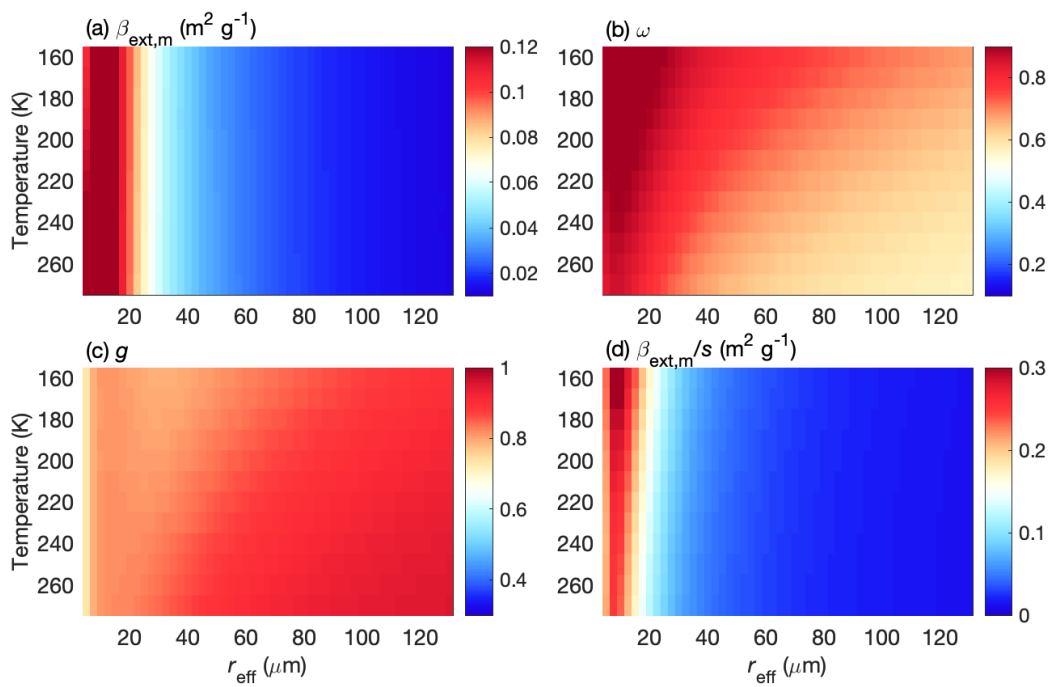Figure S9. Same as Figure S7 except at the wavenumber of 314 cm^{-1} (or $\lambda = 31.8425$ μm).

Figure S10. Same as Figure S7 except at the wavenumber of 451 cm^{-1} (or $\lambda = 22.1825$ μm).

Table S1. BT simulation experiments

Experiments	Layer cloud bulk optical properties at each wavenumber
control	Obtained via linear interpolations in both the wavenumber and temperature dimensions
160K	Obtained via linear interpolation in the wavenumber dimension only at the minimum available temperature of 160 K
270K	Obtained via linear interpolation in the wavenumber dimension only at the maximum available temperature of 270 K